Mesoporous TiO_2: Comparison of Classical Sol–Gel and Nanoparticle Based Photoelectrodes for the Water Splitting Reaction

Pascal Hartmann,[†] Doh-Kwon Lee,[‡] Bernd M. Smarsly,[†] and Juergen Janek[†,*]

[†]Physikalisch-Chemisches Institut, Justus Liebig University, Giessen Heinrich-Buff-Ring 58, 35392 Giessen, Germany, and [‡]Solar Cell Center, Korea Institute of Science and Technology (KIST), Seoul, 136-791, Korea

ABSTRACT This paper describes a systematic comparison of the photoelectrochemical properties of mesoporous TiO_2 films prepared by the two most prevalent templating methods: The use of preformed, crystalline nanoparticles is generally considered advantageous compared to the usage of molecular precursors such as $TiCl_4$, since the latter requires a separate heat treatment at elevated temperature to induce crystallization. However, our photoelectrochemical experiments clearly show that sol–gel derived mesoporous TiO_2 films cause an about 10 times higher efficiency for the water splitting reaction than their counterparts obtained from crystalline TiO_2 nanoparticles. This result indicates that for electrochemical applications the performance of nanoparticle-based metal oxide films might suffer from insufficient electronic connectivity.

KEYWORDS: photoelectrochemistry · hydrogen · titania · anatase · mesoporous · water splitting

Structuring of crystalline functional materials on the nanoscale introduces a high density of defects (surfaces and interfaces), which is often considered to be advantageous for applications requiring efficient surface reactivity, for example, photocatalytic and photoelectrochemical water splitting or sensing. Mesoporous compounds as one particular class of nanostructured materials have recently attracted strong interest, as their microstructure offers unique features: Open porosity in often hierarchical pore structures allows fast access of reactive gases and even liquids. The thin walls between these pores may show different physical properties than bulk material, and highly periodic structures provide a narrow distribution of these properties.

For these reasons, also titania (TiO_2), which plays an important role as a photocatalyst and photoelectrode base material, has been studied in mesoporous form (mp-TiO_2). mp-TiO_2 can be obtained *via* sol–gel templating, both in the form of powders and thin films. For the latter, the so-called "Evaporation-Induced self-assembly" has emerged as a versatile approach. In essence, a solution containing a TiO_2 source, a molecular Ti compound or TiO_2, a structure-directing agent (usually a block copolymer) and a volatile solvent is deposited *via* dip-coating or spin-coating. Subsequently, the films are treated at sufficiently high temperature to remove the template and to induce crystallization in the case of films based on molecular TiO_2 precursors.[1] In most cases, the anatase modification was studied, since the synthesis of high surface, mesoporous TiO_2 rutile films still remains a challenge.[2]

In recent years, the usage of preformed, crystalline oxide nanoparticles was proposed as superior toward the usage of molecular precursors ($TiCl_4$, *etc.*), in that no separate, temperature-induced crystallization step is required which can potentially disrupt the mesostructure. Although so far already a number of metal oxides can be prepared using preformed oxide nanoparticles, surprisingly only limited data are available regarding the differences in fundamental physical properties of these two types of synthetic approaches. In the present paper, we compare the properties of these two types of mp-TiO_2 films, prepared by a conventional sol–gel route and by a nanoparticle-based route, and their performance as photoelectrodes for the splitting of water. Since the first reports on TiO_2 as a photoanode for the light-driven decomposition of water by Fujishima and Honda,[3] numerous studies on the improvement of water splitting efficiency have been reported, for example, band tailoring by doping the titanium[4,5] or the oxygen sublattice[6–8] in order to gain visible light

*Address correspondence to juergen.janek@phys.chemie.uni-giessen.de.

Received for review March 9, 2010 and accepted May 12, 2010.

Published online May 20, 2010.
10.1021/nn1004765

photoresponse. Other approaches are based on increasing the surface area by nanostructuring[9] or the use of TiO_2 based composite materials.[10,11]

Mesoporous TiO_2 has already been studied in the form of dispersed particles for photocatalytic hydrogen evolution by Sreethawong *et al.*[2] Augustynski *et al.* systematically studied nanocrystalline and porous TiO_2 photoelectrodes prepared of commercial TiO_2 powders (Degussa P25).[12,13]

However, to our knowledge, there is yet no study available on mesoporous TiO_2 thin film electrodes focusing on a clear correlation between preparation, microstructure, and photoelectrochemical water splitting efficiency. A recent study on the mesoporous thin film systems, which are similar to the materials investigated in this work, used for electrochemical capacitors by Brezesinski *et al.*[14] shows a significant capacitance advantage of nanoparticles films due to a higher specific surface area. Also, recently Szeifert *et al.* introduced a "brick and mortar" strategy by mixing preformed titania nanoparticles with surfactant-templated sol−gel titania in order to achieve (partial) crystalline films at very mild conditions.[15]

Efficiency of Water Photoelectrolysis. Proper determination of the efficiency concerning the light to chemical energy conversion is critical in evaluating the performance of a photoelectrode. Different strategies have been suggested and employed for its determination. A detailed review on efficiency calculations for water photoelectrolysis cells is given by Varghese *et al.*[16] In the present work, the two most common ways of efficiency estimation are adopted as introduced below:

The so-called *conversion efficiency* is defined as the ratio between energy gained due to the formation of hydrogen and oxygen and the energy input due to illumination and electrical biasing. The energy that is stored during hydrogen production is given by the standard Gibbs free energy $\Delta_r G_m^\circ = 273.2\ \mathrm{kJ \cdot mol^{-1}}$ of the water-splitting reaction (referred to 1 mol of water). In case of PEC experiments, the transferred charge carriers, given by the integration of the photocurrent I_{ph} over the illumination time t, are measured instead of the amount of generated hydrogen. Then, the relation between the gain of chemical energy E_{chem}, $\Delta_r G^\circ$ and I_{ph} results as:

$$E_{chem} = \frac{\Delta_r G^0}{zF} I_{Ph} t \qquad (1)$$

$\Delta_r G^\circ$ divided by 2 times the Faraday constant F is better known as the value 1.229V, the standard cell voltage of the water splitting reaction. Assuming 100% Faradaic conversion, that is, that all charge carriers are utilized only for the generation of H_2, and taking into account that applying an external bias U_{appl} to the photoelectrochemical cell (PEC) costs electrical energy, the conversion efficiency η_{CE} is given by

$$\eta_{CE} = \frac{I_{ph}(1.229V - U_{appl})}{P_{irr}} \qquad (2)$$

with P_{irr} denoting the irradiation power at the photoelectrode. The highest reported conversion efficiency values up until now are 16.25% for TiO_2 nanotube arrays[17] (biased) and 12.4% for a III−V semiconductor multilayer electrode (unbiased).[18] In ref 17, only a limited range of wavelengths was used (320−400 nm), so that one has to be careful in comparing them with other results.

Beside the efficiency of power conversion, the *external quantum efficiency* η_{QE} or *incident photon-to-current efficiency* (IPCE) is used to describe the performance of photoelectrodes. In this case, the ratio between the numbers of incident photons $\#_{ph}$ and generated electronic charge carriers $I_{Ph}t/e_0$ gives η_{QE}. To quantify $\#_{ph}$, it is beneficial to use monochromatic light with a chosen wavelength λ instead of white light. Then, the expression of the IPCE for a given wavelength λ reads

$$\mathrm{IPCE} = \frac{hcI_{ph}}{e_0 \lambda P_{irr}} \qquad (3)$$

As the conversion efficiency strongly depends on the spectrum of the used light source and IPCE depends on the applied external bias, a comparison of values published in literature is meaningless without the precise knowledge of the experimental conditions. For instance, the use of a reference electrode in a three electrode setup offers the exclusive evaluation of processes at the photoelectrode. Processes occurring at the counter electrode are neglected although unavoidable overpotentials lead to an additional loss in efficiency. Just recently Maschmeyer *et al.* complained about a deficiency of standardized characterization procedures in the field of solar hydrogen generation. Therefore, the authors critized that achieved results for different material systems are hardly comparable.[19]

RESULTS

Photoelectrochemistry. Figure 1 shows the $I-U$ characteristics of the mp-TiO_2 films prepared on FTO substrates. Measurements were carried out with a scan rate of 2 mV/s. Both samples show an open cell volt-

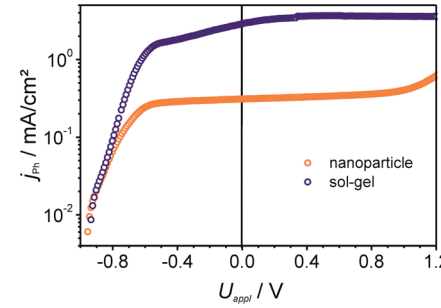

Figure 1. $I-U$-characteristics of mp-TiO_2 photoelectrodes under illumination (ca. 1000 mW/cm²). The dark currents are shown in the Supporting Information (Figure S1).

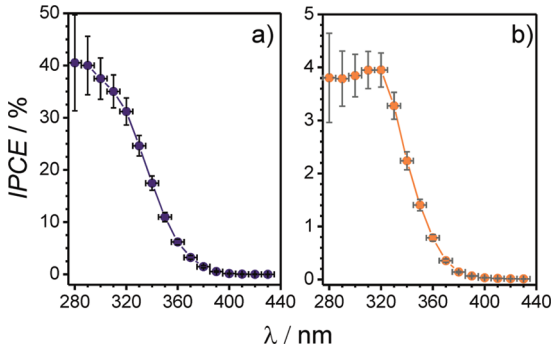

Figure 2. Quantum efficiency (IPCE) of sol−gel (a) and nanoparticle films (b) at $U_{appl} = 0$ V. The point connecting lines are only for eye guidance. The measured values for light intensities and photocurrents as function of the wavelength can be found in Figure S2.

age U_{oc} of about −0.95 V (under steady state conditions about 0.85 V) and a steep increase of photocurrent density j_{ph} with increasing applied voltage U_{appl}. Between −0.5 V and +1.0 V, the photocurrent of the nanoparticle film rises little, whereas in the case of sol−gel films, j_{ph} increases significantly up to +0.3 V. The short circuit current densities are 2.89 mA/cm^2 and 0.32 mA/cm^2 and maximum values for j_{ph} are 3.5 mA/cm^2 and 0.35 mA/cm^2 for sol−gel and nanoparticle films, respectively. The step at +0.35 V in the *I*−*U* curve of the sol−gel sample is an experimental artifact. The maximum conversion efficiency is calculated using eq 1. We obtain about 0.36% at 0 V for the sol−gel film and 0.04% at 0 V for the nanoparticle film.

Assuming ideal monochromatic light and complete Faradaic conversion, IPCE values can be calculated from the photocurrent response for each wavelength (Figure 2). Both samples show notable IPCEs for wavelengths of about 390 nm or shorter. At 320 nm, the nanoparticle-based samples already reached the maximum efficiency of 4%, whereas the sol−gel samples show an increase in efficiency up to 40% for the lowest measured wavelength. The large error bars at small wavelengths are due to the low fraction of UV light in the light source spectrum and therefore a high uncertainty of the intensity measurement. The error calculations include the spectral bandwidth of the monochromator as well as the uncertainty of light intensity and current measurements.

A simple estimate of the mean IPCE for the spectral range used in ref 17 (320−400 nm) with our data for the sol−gel electrode results in almost 12% efficiency which is not too far away from the data (16.25%) in that reference.

Optical Properties. Significant light absorption of the TiO_2 films starts at approximately 380 nm reaching a plateau at about 320 nm where up to 90% of the incident light is absorbed (not shown in the graph). To determine the materials band gap energy E_g, the square root of the measured absorption coefficient as function of the photon energy is shown in Figure 3. TiO_2 is considered as an indirect semiconductor, and thus, the optical absorption coefficient α is expected to show a square root dependence for the photon energy $h\nu$ near the band gap energy E_g:[20]

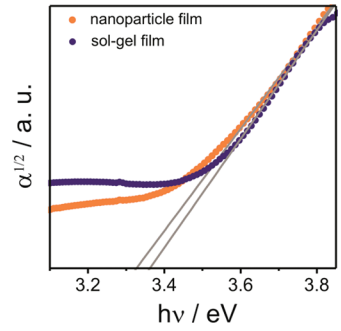

Figure 3. Determination of the band gap energy E_g for sol−gel and nanoparticle based films from absorption spectra. According to the indirect optical band gap in TiO_2, the square root of the absorption coefficient is plotted *vs* the photon energy and E_g is estimated by linear approximation of the absorption edge to $\alpha = 0$.

$$\alpha \propto (h\nu - E_g)^{1/2}, \quad h\nu > E_g \qquad (4)$$

E_g is evaluated as 3.3−3.4 eV for the mp-TiO_2 films. These results are in good agreement with values published by Wong *et al.* who characterized interband transitions of anatase films deposited by electron beam evaporation by thermoreflectance spectroscopy.[21] Other studies, both experimental and theoretical, lead to the conclusion that (nanocrystalline) anatase shows a direct absorption edge.[22,23] Therefore, we also plotted α^2 *versus* $h\nu$ obtaining bandgap energies of 3.6−3.7 eV for a direct transition (Figure S3).

Morphology and Structure. Figure 4 shows SEM images of the mp-TiO_2 electrodes. Both films show a regular mesoporosity with a pore diameter of about 15 nm and a high film quality with large crack free areas, as reported in literature[14] (not shown in the pictures). The pore structure of the nanoparticle films is more open (*i.e.*, it shows a higher density of accessible pores at the surface) than the sol−gel samples. Films prepared by the sol−gel process have a significantly thicker TiO_2 framework possessing about 15 nm thick pore walls compared to 7 to 8 nm thick walls of the nanoparticle films. The thicknesses of sol−gel and nanoparticle films

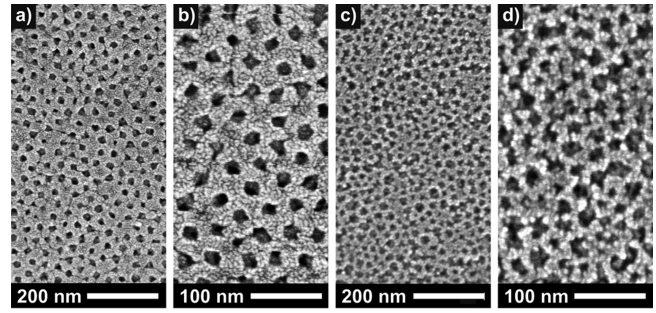

Figure 4. HRSEM images of mp-TiO_2 thin films prepared (a and b) by the sol−gel route and (c and d) by the nanoparticle route.

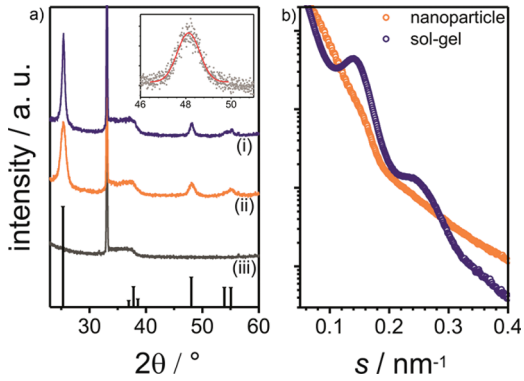

Figure 5. (a) Wide angle X-ray diffraction patterns (Cu Kα source) of sol−gel (i) and nanoparticle films (ii) on silicon substrates (iii) are shown. The Bragg reflections for an ideal anatase powder pattern are indicated as vertical bars at the bottom of the graph. The small inset shows a pseudo-Voigt fit of one of the measured peaks. (b) Small angle X-ray scattering patterns of sol−gel (blue circles) and nanoparticle (orange circles) films prepared on silicon wafers and calcined at 300 °C.

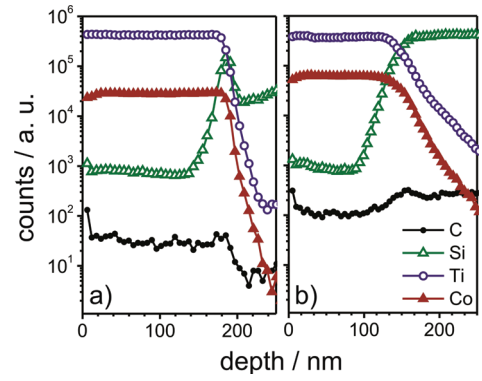

Figure 6. Depth profiles of sol−gel (a) and nanoparticle films (b) as determined by ToF-SIMS. The pore system was impregnated with a cobalt salt solution in order to prove electrolyte accessibility. Only the signals of positively single charged ions are shown. The point connecting lines are only for eye guidance.

are determined by profilometry as (185 ± 21) and (144 ± 8) nm, respectively.

Wide angle X-ray diffraction (Figure 5 a) was carried out with mesoporous films on highly oxidized silicon substrates, to reduce substrate scattering. Identification of the main peaks and relative intensities was found to match the anatase phase according to JCPDS reference card no. 21-1272, and reflections of other TiO_x phases could not be observed. To estimate the average crystallite size, we evaluated the width (fwhm) of the strongest reflections (2θ: 25.3°, 48.03°) using the Scherrer equation.[24] We obtained 9−11 and 16−17 nm for the nanoparticle and sol−gel films, respectively, confirming the analysis of SEM images. Figure 5b shows 1D SAXS curves measured in symmetric reflection obtained with films on silicon wafers calcined at 300 °C. 2θ ranges from 0.5° to 4.5°, and s is the scattering vector: $s = 2\sin(\theta)/\lambda$. The sol−gel films show distinct scattering maxima at $s = 0.14$ nm^{-1} and $s = 0.24$ nm^{-1} which indicate an ordered mesoporous system with cubic structure, as typically observed for PIB templated sol−gel films, but with a certain degree of distortion.[25] The SAXS curves of the nanoparticle films do not show any feature indicating an ordered system of mesopores. The apparent discrepancy with the SEM figures is probably due to the fact that the mesopores themselves still do possess a well-defined shape, but show a high degree of positional disorder as a consequence of the stress during the reorganization of the nanoparticles.

To obtain information about the electrolyte accessibility, we infiltrated the mp films with a tracer solution of cobalt nitrate. After drying, depth profiles were measured in order to resolve the Co concentration within the TiO_2 structure (Figure 6). It can be seen that for both films the Co and the Ti concentration is almost constant until reaching the Si wafer used as substrate which is indicated by a steep increase of the Si signal. The delay between rise of the Si signal and drop of the Co and Ti signals is caused by ion mixing effects typical of ToF-SIMS.

DISCUSSION

Morphology and Structure. According to their morphology, both types of samples may have different advantages with respect to the photoelectrochemical performance. The more open pore structure of the nanoparticle samples gives rise to high electrolyte accessibility and, therefore, fast transport of the reacting species. Furthermore, the nanoparticle films (350−400 m^2/g) have an about 2 times larger specific surface area than the sol−gel derived films (180−200 m^2/g) as determined by Brezesinski *et al. via* toluene physisorption combined with gravimetric measurements (those films were templated with a different block copolymer (KLE), which leads to a comparable pore structure).[14] On the other hand, the sol−gel samples should instead show better electronic transport properties due to both the relatively thick TiO_2 framework and the about 60% larger crystallites. Kim *et al.* investigated the photocatalytic activity of nanostructured TiO_2 focusing on the influence of the nanoparticles morphology.[26] They observed the lowest activity for spherical particles even though those feature the highest surface area. Mixing spherical and rod-like particles leads to a significant enhancement which Kim *et al.* explained with improved electronic transport established by the rod-like nanocrystals and their anisotropic shape. In a recent study on single crystalline TiO_2 nano pillar arrays, Dong *et al.* ascribed a superior photoelectrochemical performance to a low fraction of grain boundaries and direct electronic pathways.[9]

The sol−gel samples seem to form a continuous TiO_2 network, whereas the connection between nanoparticles surrounding the pores seems to be less continuous. The latter leads to a reduced density of conduction paths for charge carriers within the

nanopoarticle-templated film. To explain this finding, it is necessary to consider the synthesis of mesoporous films using block-copolymers *via* evaporation-induced self-assembly (EISA process).[27,28] The block copolymers assemble to a periodic system of micelles, that is, to a lyotropic liquid crystal phase. The dimensions of the micelles are basically given by the molecular structure and concentration of the used polymer. The metal oxide is then built around the micelles either by hydrolysis and condensation reactions of molecular precursors or by destabilization of a colloidal solution of nanoparticles. The dimension of a molecular precursor is usually negligible compared to a 15 nm micelle and the built amorphous TiO_2 network is flexible up to a certain degree of condensation and can easily match within the organic liquid crystal structure. In contrast, the presynthesized TiO_2 nanoparticles are about 7 to 8 nm in diameter[29,30] and rigid. Thus, the assembly of nanoparticles and micelles to a somehow closed package can locally lead to a distorted structure and discontinuous pore walls (template−particle size mismatch). To avoid these local distortions, it is beneficial to use smaller nanoparticles, but the use of smaller particles leads to a lower photoelectrochemical performance.

As SEM images mainly contain surface information, we carried out small-angle X-ray scattering experiments on the TiO_2 films to get volume information on the mesoscopic scale, when the block-copolymer is still inside the pores. For the sol−gel films, we observed significant scattering maxima, whereas we observed no such features for nanoparticles. This finding confirms that the nanoparticle/block-copolymer system tends to mesoscopic disorder to compensate the template−particle size mismatch. It has to be noted that heating to 550 °C (within 50 min, starting at 300 °C) results in a complete loss of the scattering maxima indicating a loss of ordering due to crystal growth within the pore walls. Indeed the ordered structure of the sol−gel films could be preserved to the point of crystallization using a faster heating ramp (30 min); however, those samples showed a lower performance as PEC electrodes.

In the above-mentioned "brick and mortar" approach, Szeifert and co-workers[15] synthesized mesoporous TiO_2 thin films at very mild conditions (calcination at max. 300 °C) by mixing preformed crystalline nanoparticles (bricks) with a templated sol−gel titania (mortar). They investigated both the photocatalytic (NO oxidation) and photoelectrochemical (DSSC electrode) performance as function of the film particle content. For both applications, mixtures with about 60−80% particle content gained highest and pure sol−gel films lowest efficiencies. The latter seems to contradict our results, but can be explained by the different temperature treatments: As shown in an earlier work,[31] sol−gel derived TiO_2 films show almost no crystallinity up to 400−450 °C (depending on the used template). Therefore, in this work, all samples were calcined at 550 °C to obtain TiO_2 with high crystallinity. The benefit of mixtures is related to both a certain degree of crystallinity introduced by the particles and a good particle interconnection *via* the sol−gel titania "glue". In good agreement with our results, films with 100% particle content show a significant decrease in efficiency compared to the mixed films. The authors relate this observation to insufficient sintering *via* solid state diffusion of particles at 300 °C. Our results show that even 550 °C are not enough to achieve an interparticular sintering which would provides sufficiently conductive charge transport paths.

Optical Properties. Both sample types show quite comparable absorption behavior. The band gap energies of 3.3−3.4 eV are only a little higher than 3.2 eV for bulk TiO_2 (anatase modification).[32] It is well-known that the decrease of the crystallite size can alter optical properties of a semiconductor material. Below a certain dimension, electronic states get confined, resulting in a blue shift of the band gap energy.[33] But the discrepancy of 0.1−0.2 eV can simply be the result of the experimental uncertainty.

As the wavelength resolved IPCE values give information on the absorption properties of the photoelectrodes, it is useful to take a closer look at these results converting the light wavelengths into photon energies. The IPCE increases for photon energies around 3.3 eV which is in good agreement with the obtained values for an indirect band gap (Figure S4). Without using more sophisticated techniques to analyze the optical/electronic properties, it is not possible to give more precise information at this point.

Photoelectrochemistry. Both samples have conversion efficiencies far below 1.7%, that is, the theoretical maximum efficiency for photoelectrochemical water splitting using a semiconductor with a band gap of 3.2 eV like anatase phase TiO_2 and the full spectrum of a Xe-arc light source.[16] However, the mesoporous photoelectrodes gain almost maximum conversion efficiency without applying an external voltage. Thinking of applications for solar hydrogen generation, the expendability of an electrical power source would offer low-end systems and installation aloof electricity networks. Mishra *et al.* reported conversion efficiencies of more than 2% for spin coated TiO_2 films on Ti substrates biased with about 600 mV but only negligible values (<0.1%) without biasing the photoelectrodes.[34] For hematite (α-Fe_2O_3) electrodes, Grätzel *et al.* reported significant photocurrents only for potentials <0.8 V *versus* RHE.[35] In a recent work, Wolcott *et al.* investigated ZnO photoelectrodes and obtained conversion efficiencies between 0.1% and 0.6% (depending on the preparation method) under 1 V bias.[36] At this point, it has to be mentioned that in refs 34−36 light sources different from ours were used, and therefore, a comparison of the absolute efficiency values is not possible. Further, we evaluated the efficiency of the whole PEC, whereas in

the quoted contributions, a three electrode setup was used.

By optimizing both the photoelectrodes and the experimental setup, it should be possible to obtain higher efficiency values, as the optimum thickness for nanostructured anatase films should be in the μm range. For experimental reasons, we were not able to use lower illumination intensities. This might be another interesting point for future studies, as Ooms and co-workers demonstrated a high intensity dependence of the conversion efficiency at La_2CuO_4 electrodes, ranging from about 1% (45 mW/cm^2) to 0.2% (1600 mW/cm^2).[37]

The comparison of the two types of mp-TiO_2 photoelectrodes illustrates that the nanoparticle films show roughly 10 times lower conversion and quantum efficiencies than the sol−gel films, although the preparation route for both types of films is quite similar. To exclude differences in film thickness as a reason for large differences in PEC performance, we investigated sol−gel samples with varying film thickness. Even a 100 nm thick film shows 7 times higher photocurrents and efficiencies than the 144 nm thick nanoparticle film.

As already indicated above, the different morphology of the TiO_2 framework may cause these enormous discrepancies. The early IPCE saturation at low bias ($U_{appl} = 0$ V) for nanoparticles may be caused by recombination of photogenerated charge carriers. Augustynski *et al.* investigated the influence of molecular oxygen dissolved in the electrolyte on the photoelectrochemical performance of mesoporous TiO_2 electrodes.[38] They found that for small wavelengths the IPCE values significantly drop for an oxygen saturated electrolyte and related this effect to the decreasing light penetration depth with decreasing wavelength. Using the absorption coefficients for titania measured by Eagles,[39] Augustynski *et al.* estimated a penetration depth of 30 nm and 3 μm for wavelength of 300 and 380 nm, respectively, in case of a mp-TiO_2 film.[40] At higher photon energies, electron hole pairs are generated near the electrode surface resulting in a longer conduction path length across the mesoporous structure. This facilitates a higher recombination probability due to the electrolyte filled pore structure.

As there is no significant difference in the optical properties, crystallographic structure, as well as electrolyte accessibility, we relate the discrepancy in the photoelectrochemical performance to electronic transport within the mesoporous TiO_2 (Figure 7). (1) The spherical shape of the nanoparticles intrinsically leads to a loose connection between particles (constriction resistance) and a low electronic conductivity of the film. (2) The smaller dimension of the pore walls and crystallites leads to a higher recombination probability of electrons and holes within a single particle and at the grain boundaries. Because of the higher specific surface area of the nanoparticle films, the recombination of photogenerated electrons with an oxidized species in the electrolyte is also facilitated. (3) The template−particle size mismatch leads to discontinuous TiO_2 pore walls and, therefore, to a lower fraction of conduction pathways within the film.

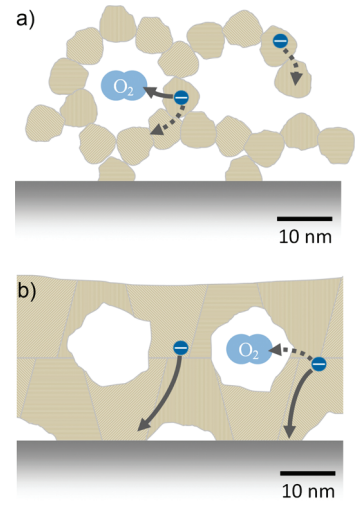

Figure 7. Sketch of the electronic transport within the mesoporous photoelectrodes. (a) The small nanoparticles and the template−particle size mismatch result in a low conduction path cross section. Recombination with, *e.g.*, dissolved oxygen is facilitated due to the high surface area. (b) The sol−gel films therefore show high photo currents due to thick and continuous pore walls and a lower recombination rate.

CONCLUSION

In summary, mesoporous TiO_2 films were synthesized by two widely used approaches regarding the precursor of TiO_2 (molecular compounds such as $TiCl_4$ and preformed crystalline TiO_2 nanoparticles) and studied regarding their photoelectrochemical properties. In principle, using preformed crystalline nanoparticles is generally considered to be advantageous, circumventing the synthetic problems of molecular precursors: In case of the sol−gel route, one has to use a reactive solution containing titanium compounds, the hydrolysis and condensation of which are difficult to control. Also, high temperatures are required to achieve the transformation into the crystalline oxide, potentially disrupting the mesoporosity. In our studies, the sol-based mesoporous TiO_2 films appeared to be superior with respect to photoelectrochemical properties as model system. The present study thus questions the paradigmatic assumption that the usage of preformed metal oxide nanoparticles is fundamentally superior over mesoporous films prepared from molecular precursors. By contrast, the electronic connectivity of the oxidic matrix is of crucial importance.

The present study could not address the question whether the low connectivity observed for particle-based films is just due to the fact that the nanoparticles used are small. For such investigations, significantly larger nanoparticles are required (*ca.*

20 nm in diameter), which however are incommensurate with the block copolymers used. Future studies will be dedicated to the use of larger block copolymer micelles and further details of the differences in the electronic transport of other mesoporous metal oxides.

EXPERIMENTAL METHODS

Film Preparation. The synthetic route for the film preparation is adopted from Brezesinski *et al.*[14]

Sol−gel Route. Approximately 0.3 mL of titanium tetrachloride (<98%, Fluka) was mixed with 3 g of ethanol (99,8%, VWR) under vigorous stirring. In a second vessel, 110 mg of PIB3000 (BASF SE, Ludwigshafen, Germany) was dissolved in 2.5 g of ethanol using an ultrasonic bath. After 30 min, both solutions were mixed together with 0.4 mg of water.

Nanoparticles. One milliliter of $TiCl_4$ was carefully added to 5 g of ethanol, stirred for 5 min, and was then combined with 20 g of benzyl alcohol (99%, Merck) and 240 mg of 1.3-propanediol (99%, Alfa Aeser). The solution was stirred for 8 h at 80 °C. To isolate the obtained particles, the transparent solution was given to *ca.* 200 mL of diethyl ether (99%, Merck) and centrifuged at 3500 rpm for 10 min. The white precipitate was dried at room temperature (RT) for 1 h and then dispersed in about 3 mL of ethanol and 0.3 mL of double distilled water. Afterward, 110 mg of PIB3000 was dissolved in the nanoparticle dispersion and sonicated for 20 min.

Film Deposition. All samples are prepared as thin films on different substrates (Si, SiO_2, FTO glass) using a dip-coating technique. Optimal coating conditions include filtering of the solutions with 0.2 μm micro filters, 20% of relative humidity for the sol−gel samples and 80% for the nanoparticle-based samples, as well as a constant withdrawal rate varying from 3 to 13 mm/s.

During drying of the wet coating, the so-called evaporation induced self-assembly (EISA) process of the amphiphilic block copolymer PIB3000 took place. This resulted in an ordered arrangement of spherical mesopores in the titania matrix (see ref 26 for a review of the preparation on mesoporous materials by using block copolymers).

The films were dried in air at 100 °C for 1 h and aged at 300 °C for 12 h. To remove the organic template and crystallize the titania framework, samples were heated from 300 to 550 °C within 50 min and kept for 5 min at this temperature. Longer heating was avoided as it may cause the collapse of the metastable porous network. All temperature treatments were carried out in a commercial muffle furnace (Nabertherm L 3/11/P320).

Characterization. *Scanning electron microscopic images* were taken with a LEO Gemini 982 high resolution SEM (field emission gun). All samples for the SEM experiments were prepared on (100) single crystal silicon. *Wide angle X-ray diffraction* and *small-angle X-ray scattering* experiments were done in θ−2θ geometry on a Panalytcal X'Pert diffractometer with Cu Kα source (40 kV, 40 A). *Scherrer Analysis*: for fitting the wide angle reflections, we used a pseudo-Voigt function of the Originlab Origin 8.0 software. For nanometer-sized primary particles (average diameter *ca.* 10 nm), the corresponding peak widths in WAXS data are mainly determined by the crystallite size, so that the influence of instrumental broadening could be neglected. The film thickness was measured by a *profilometer* (Alpha-step IQ). The spatial homogeneity of the chemical composition of the samples was analyzed by a *time-of-flight secondary ion mass spectrometer* (Fa. Ion TOF 5) equipped with a bismuth gun for analysis. In this work, the spectra of positively charged ions are used. For depth profiling, the films were sputtered using a O_2 gun (1 kV, 14.4 nA, 5 s sputter time) supported by an electron flood gun to avoid electric charging of the samples. To investigate the accessibility of the porous microstructure of the films, we preimpregnated them with a 10^{-4} M $Co(NO_3)_2$ tracer solution before analyzing. The dimensions of the sputtered craters were about 100 × 100 μm^2, whereas the chemical analyses were done on a area of about 25 × 25 μm^2. The optical properties were determined with an *UV−vis-IR Spectrometer* (UVIKON Lambda 900) measuring the wavelength dependence of reflection and transmission coefficients (step width of 1 nm and a scan rate of 150 nm/min). In this case, silica glass (*ca.* 10 × 20 × 2 mm^3) was used as substrate. An uncoated quartz substrate and an aluminum mirror were used as references for transmission and reflection measurements, respectively. The *photoelectrochemical experiments* were carried out in a rectangular PMMA reactor (*ca.* 30 × 50 × 100 mm^3) equipped with a quartz window. A two-electrode system was used: a platinum foil counter electrode (300 mm^2) and the mp-TiO_2 electrodes (19.6 mm^2) immersed in an aqueous 0.1 M NaOH electrolyte. For the PEC measurements, the TiO_2 films were coated on commercial FTO glass substrates. Bias supply and current measurements were done by an electrochemical workstation (Zahner IM 6). As light source, we used a 150 W Xe Arc lamp (Lot Oriel) and a Thermopile (OPHIR 1Z02662) plus Powermeter (Nova Oriel) for light intensity measurements. The *quantum efficiency* or incident photon to charge carrier conversion efficiency (IPCE) was measured by illuminating the samples with monochromatic light beam (monochromator, Lot Oriel, MSH101, width of entrance and exit slit: 2.5 mm). The photocurrent at each wavelength was recorded until the steady state at a constant electrode potential of 0 V was observed (Zahner IM 6).

Acknowledgment. The Authors thank S. O. Steinmüller for SIMS measurements and D. Reppin and B. K. Meyer for the optical characterization. Further, the authors thank D. Schlettwein for his ideas and advice.

Supporting Information Available: Four additional charts: *I−U* curves without illumination, raw data for IPCE calculation, direct optical absorption curve and IPCE *vs* photon energy. This material is available free of charge *via* the Internet at http://pubs.acs.org.

REFERENCES AND NOTES

1. Smarsly, B.; Grosso, D.; Brezesinski, T.; Pinna, N.; Boissière, C.; Antonietti, M.; Sanchez, C. Highly Crystalline Cubic Mesoporous TiO_2 with 10-nm Pore Diameter Made with a New Block Copolymer Template. *Chem. Mater.* **2004**, *16*, 2948–2952.
2. Sreethawong, T.; Suszuki, J.; Yoshikawa, S. Synthesis, Characterization, And Photocatalytic Activity for Hydrogen Evolution of Nanocrystalline Mesoporous Titania Prepared by Surfactant-Assisted Templating Sol-Gel Process. *J. Solid State Chem.* **2005**, *178*, 329–338.
3. Fujishima, A.; Honda, K. Electrochemical Photolysis of Water at a Semiconductor Electrode. *Nature* **1972**, *238*, 37–38.
4. Hermann, J.-M.; Mozzanega, M.-N.; Pichat, P. Oxidation of Oxalic Acid in Aqueous Suspensions of Semiconductors Illuminated with UV or Visible Light. *J. Photochem.* **1983**, *22*, 333–343.
5. Serpone, N.; Lawless, D.; Disdier, J.; Hermann, J.-M. Spectroscopic, Photoconductivity, And Photocatalytic Studies of TiO_2 Colloids: Naked and with the Lattice Doped with Cr^{3+}, Fe^{3+}, and V^{5+} Cations. *Langmuir* **1994**, *10*, 643–652.
6. Sato, S. Photocatalytic Activity of NO_x-Doped TiO_2 in the Visible Light Region. *Chem. Phys. Lett.* **1986**, *123*, 126–128.
7. Khan, S. U. M.; Al-Shahry, M.; Ingler Jr., W. B. Efficient Photochemical Water Splitting by a Chemically Modified n-TiO_2. *Science* **2002**, *297*, 2243–2245.
8. Nagaveni, K.; Hegde, M. S.; Ravishankar, N.; Subbanna, G. N.; Madras, G. Synthesis and Structure of Nanocrystalline TiO_2 with Lower Band Gap Showing High Photocatalytic Activity. *Langmuir* **2004**, *20*, 2900–2907.
9. Dong, X.; Tao, J.; Li, Y.; Zhu, H. Oriented Single Crystalline TiO_2 Nano-Pillar Arrays Directly Grown on Titanium

Substrate in Tetramethylammonium Hydroxide Solution. *Appl. Surf. Sci.* **2010**, *256*, 2532–2538.
10. Takabayashi, S.; Nakamura, R.; Nakato, Y. A Nano-Modified Si/TiO_2 Composite Electrode for Efficient Solar Water Splitting. *J. Photochem. Photobiol. A* **2004**, *166*, 107–113.
11. Zhang, J.; Bang, J. H.; Tang, C.; Kamat, P. V. Tailored TiO_2-$SrTiO_3$ Heterostructure Nanotube Arrays for Improved Photoelectrochemical Performance. *ACS Nano* **2010**, *4*, 387–395.
12. Morand, R.; Lopez, C.; Hep-Koudelka, M.; Kedzierzawski, P.; Augustynksi, J. Photoelectrochemical Behavior in Low-Conductivity Media of Nanostructured TiO_2 Films Deposited on Interdigitated Microelectrode Arrays. *J. Phys. Chem. B* **2002**, *106*, 7218–7224.
13. Solarska, R.; Augustynski, J.; Sayama, K. Viewing Nanocrystalline TiO_2 Photoelectrodes As Three-Dimensional Electrodes: Effect of the Electrolyte upon the Photocurrent Efficiency. *Electrochim. Acta* **2006**, *52*, 694–703.
14. Brezesinski, T.; Wang, J.; Polleux, J.; Dunn, B.; Tolbert, S. H. Templated Nanocrystal-Based Porous TiO_2 Films for Next-Generation Electrochemical Capacitors. *J. Am. Chem. Soc.* **2009**, *131*, 1802–1809.
15. Szeifert, J. M.; Fattakhova-Rohling, D.; Georgiadou, D.; Kalousek, V.; Rathousky, J.; Kuang, D.; Wenger, S.; Zakeeruddin, S. M.; Grätzel, M.; Bein, T. "Brick and Mortar" Strategy for the Formation of Highly Crystalline Mesoporous Titania Films from Nanocrystalline Building Blocks. *Chem. Mater.* **2009**, *21*, 1260–1265.
16. Varghese, O. K.; Crimes, G. A. Appropriate Strategies for Determining the Photoconversion Efficiency of Water Photoelectrolysis Cells: A Review with Examples Using Titania Nanotube Array Photoanodes. *Sol. Energy Mater. Sol. Cells* **2008**, *92*, 374–384.
17. Paulose, M.; Shankar, K.; Yoriya, S.; Prakasam, H. E.; Varghese, O. K.; Mor, G. K.; Latempa, T. A.; Fitzgerald, A. Anodic Growth of Highly Ordered TiO_2 Nanotube Arrays to 134 μm in Length. *J. Phys. Chem. B* **2006**, *110*, 16179–16184.
18. Khaselev, O.; Turner, J. A. A monolithic Photovoltaic-Photoelectrochemical Device for Hydrogen Production *via* Water Splitting. *Science* **1998**, *280*, 425–427.
19. Maschmeyer, T.; Michel, C. Catalytic Aspects of Light-Induced Hydrogen Generation in Water with TiO_2 and Other Photocatalysts: A Simple and Practical Way Towards a Normalization. *Angew. Chem., Int. Ed.* **2010**, *49*, 1536–1539.
20. Yu, P. Y., Cardona, M. *Fundamentals of Semiconductors Physics and Materials Properties*, 3rd ed.; Springer: Berlin, Heidelberg, New York, 2005; pp 268−276.
21. Ho, C.-H.; Tsai, M.-C.; Wong, M.-S. Characterization of Indirect and Direct Interband Transitions of Anatase TiO_2 by Thermoreflectance Spectroscopy. *Appl. Phys. Lett.* **2008**, *93*, 081904.
22. Serpone, N.; Lawless, D.; Khairutdinov, R. Size Effects on the Photophysical Properties of Colloidal Anatase TiO_2 Particles: Size Quantization or Direct Transitions in This Indirect Semiconductor. *J. Phys. Chem.* **1995**, *99*, 16646–16654.
23. Asahi, R.; Taga, Y.; Mannstadt, W.; Freeman, A. J. Electronic and Optical Properties of Anatase TiO_2. *Phys. Rev. B* **2000**, *61*, 7459–7465.
24. Patterson, A. L. The Scherrer Formula for X-Ray Particle Size Determination. *Phys. Rev.* **1939**, *56*, 978–982.
25. Wang, Y.; Brezesinski, T.; Antonietti, M.; Smarsly, B. Ordered mesoporous Sb-, Nb-, and Ta-Doped SnO_2 Thin Films with Adjustable Doping Levels and High Electrical Conductivity. *ACS Nano* **2009**, *3*, 1373–1378.
26. Kim, J. Y.; Choi, S. B.; Kim, D. W.; Lee, S.; Jung, H. S.; Lee, J.-K.; Hong, K. S. Surfactant-Assisted Shape Evolution of Thermally Synthesized TiO_2 Nanocrystals and Their Applications to Efficient Photoelectrodes. *Langmuir* **2008**, *24*, 4316–4319.
27. Brezesinski, T.; Groenewolt, M.; Gibaud, A.; Pinna, N.; Antonietti, M.; Smarsly, B. M. Evaporation-Induced Self-Assembly (EISA) at Its Limit: Ultrathin, Crystalline Patterns by Templating of Micellar Monolayers. *Adv. Mater.* **2006**, *18*, 2260–2263.
28. Smarsly, B. M.; Antonietti, M. Block Copolymer Assemblies As Templates for the Generation of Mesoporous Inorganic Materials and Crystalline Films. *Eur. J. Inorg. Chem.* **2006**, 1111–1119.
29. Niederberger, M.; Bartl, M. H.; Stucky, G. D. Benzyl Alcohol and Titanium Tetrachlorides a Versatile Reaction System for the Nonaqueous and Low-Temperature Preparation of Crystalline and Luminescent Titania Nanoparticles. *Chem. Mater.* **2002**, *14*, 4364–4370.
30. Kotsokechagia, T.; Cellesi, F.; Thomas, A.; Niederberger, M.; Tirelli, N. Preparation of Ligand-Free TiO_2 (Anatase) Nanoparticles through a Nonaqueous Process and Their Surface Functionalization. *Langmuir* **2008**, *24*, 6988–6997.
31. Fattakhova-Rohlfing, D.; Wark, M.; Brezesinski, T.; Smarsly, B. M. Highly Organized Mesoporous TiO_2 Films with Controlled Crystallinity; A Li-Insertion Study. *Adv. Funct. Mater.* **2007**, *17*, 123–132.
32. Tang, H.; Berger, H.; Schmid, P. E.; Levy, F.; Burri, G. Photoluminescence in TiO_2 Anatase Single Crystals. *Solid State Comm.* **1993**, *87*, 847–850.
33. Ekimov, A. I.; Efros, A. L.; Onushchenko, A. A. Quantum Size Effect in Semiconductor Microcrystals. *Solid State Comm.* **1985**, *56*, 921–924.
34. Mishra, P. R.; Shukla, P. K.; Srivastava, O. N. Study of Modular PEC Solar Cells for Photoelectrochemical Splitting of Water Employing Nanostructured TiO_2 Photoelectrodes. *Int. J. Hydrogen Energy* **2007**, *32*, 1680–1685.
35. Kay, A.; Cesar, I.; Grätzel, M. New Benchmark for Water Photooxidation by Nanostructured α-Fe_2O_3 Films. *J. Am. Chem. Soc.* **2006**, *128*, 15714–15721.
36. Wolcott, A.; Smith, W. A.; Kuykendall, T. R.; Zhao, Y.; Zhang, J. Z. Photoelectrochemical Study of Nanostructured ZnO Thin Films for Hydrogen Generation from Water Splitting. *Adv. Funct. Mater.* **2009**, *19*, 1849–1856.
37. Spijker, H. v.; Dan, S.; Ooms, F. Photocatalytic Water Splitting by Means of Undoped and Doped La_2CuO_4 Photocathodes. *Int. J. Hydrogen Energy* **2008**, *33*, 6414–6419.
38. Solarska, R.; Rutkowska, I.; Augustynski, J. Unusual Photoelectrochemical Behaviour of Nanocrystalline TiO_2 Films. *Inorg. Chim. Acta* **2008**, *361*, 792–797.
39. Eagles, D. M. Polar Modes of Lattice Vibration and Polaron Coupling Constants on Rutile (TiO_2). *J. Phys. Chem. Solids* **1964**, *25*, 1243–1251.
40. Wahl, A.; Augustynski, J. Charge Carrier Transport in Nanostructured Anatase TiO_2 Films Assisted by the Self-Doping of Nanoparticles. *J. Phys. Chem. B* **1998**, *102*, 7820–7828.